Supplement of Atmos. Chem. Phys., 21, 9761–9777, 2021
https://doi.org/10.5194/acp-21-9761-2021-supplement

Atmospheric Chemistry and Physics
Open Access

Supplement of

Large seasonal and interannual variations of biogenic sulfur compounds in the Arctic atmosphere (Svalbard; 78.9° N, 11.9° E)

Sehyun Jang et al.

Correspondence to: Kitack Lee (ktl@postech.ac.kr) and Young Jun Yoon (yjyoon@kopri.re.kr)

Text.S1. Independent validation of isotope analysis using black carbon

To investigate the reliability of isotope measurement, we compared black carbon (BC) data with sulfate concentrations during the campaign periods. Arctic Haze, which originate from mostly northern Europe, consists of sulfate and other inorganic compounds, also contains black carbon resulted from incomplete combustion of fossil fuel and burning of forests (Li and Barrie, 1993; Udisti, 2016) and is one of the major source of aerosols in the Arctic during late winter to early spring (Shaw, 1995; Quinn et al., 2007). It was reported that there are similar seasonal variations and significant correlations between BC and NSS-SO_4^{2-} in the Arctic atmosphere indicating that they have common source and aging process of aerosols during meridional transport (Gong et al., 2010; Massling et al., 2015). To estimate the amount of Anth-SO_4^{2-} based on BC data, we first compared NSS-SO_4^{2-} and BC measured in March to April when the effect of Arctic Haze is most intense. Here, we assumed that all of NSS-SO_4^{2-} collected in that period would have Anth-SO_4^{2-} as dominant contributor. Furthermore, we filtered a few data points (where Bio-SO_4^{2-}/total SO_4^{2-} > 0.2) to avoid systematical bias in the calculation of the ratio between NSS-SO_4^{2-} and BC. As a result, the value of 17.3 was chosen to represent the correlation of Anth-SO_4^{2-} and BC in the Arctic Ocean and the results are shown in Fig. S1. In spite of the different location of sampling site (BC measured in Zeppelin observatory; 78.5° N, 11.8° E, 474 m above sea level), the sulfate and BC profiles matched quite well in the spring (March to May). Most of the spring time, we confirmed that those Anth-SO_4^{2-} calculated based on BC concentration and isotope analysis are similar which indicating reliability of isotope measurement. When we compare the concentration of Anth-SO_4^{2-} in summer, the difference (or relative amount of Anth-SO_4^{2-}) is getting bigger which induced by the different air mass circulation in spring and summer and also the diminishing effect of Arctic Haze in the summer, that is lower concentration of Anth-SO_4^{2-} and BC, and also different origin of air masses reflecting different ratios in Anth-SO_4^{2-} and BC. Samples with higher black carbon concentration could be originated from distant regions (i.e. not locally produced, mostly from low-latitude regions) resulted from different environmental conditions, showing different ratios.

Text.S2. Association between R_{Bio} and air temperature

At lower air temperatures DMS is oxidized more to MSA (leading to higher R_{Bio} values), whereas at higher temperatures it is oxidized more to Bio-SO_4^{2-} (leading to lower R_{Bio} values) (Hynes et al., 1986; Yin et al., 1990). For example, the values of R_{Bio} measured near the equator (where the air temperature is high) are an order of magnitude lower than the values measured at high latitudes (where air temperature is low) (e.g., Bates et al., 1992; Chen et al., 2012; Lin et al., 2012); these findings substantiate the linear dependence of the R_{Bio} on the air temperature. Equally available is evidence against the temperature dependence of R_{Bio} at given locations (Li et al., 1993; Legrand and Pasteur, 1998; Norman et al., 1999). In our study the air temperature (-1.8 ± 2.2 °C) in the distant DMS source regions (Region 2 in Fig. S10) during the pre-bloom period (March to April) was slightly lower than that (-0.1 ± 4.4 °C) during the bloom and post-bloom periods (May to August) over the local Greenland and Barents seas (Region 1 in Fig. S10), where the higher R_{Bio} values were more determined by the local DMS source. The empirical relationship between temperature and DMS oxidation products points to lower R_{Bio} values at higher air temperatures (MSA/SO_4^{2-} (%) = -1.5 × temperature (°C) + 42.2; Bates et al., 1992b). In contrast, our measurements pointed to the opposite trend, and further indicates that factors other than air temperature might be more important in the partitioning of DMS into MSA or Bio-SO_4^{2-}. Similar to our results, in other high latitude studies light intensity has been reported to be more important than air temperature in determining the seasonal variations in R_{Bio} (Gondwe et al., 2004).

Table. S1. Data points excluded for calculation of MSA to Bio-aerosol ratios (R_{Bio})

Year	Day of year	Bio-SO_4^{2-} (ng m^{-3})	MSA (ng m^{-3})	R_{Bio}
2018	80.5	0	5.55	1
	86.5	10.45	4.39	0.30
	92.5	0	12.14	1
	95.5	0	24.60	1
	98.5	14.39	8.78	0.38
	164.5	20.53	28.53	0.58
	179.5	3.13	35.91	0.92
	206.5	5.26	35.91	0.87
2019	102.1	0	23.33	1
	105.0	0	28.11	1
	108.1	0	42.28	1
	111.0	0	28.64	1
	114.0	0	43.05	1
	117.1	13.96	62.69	0.82
	120.0	23.60	48.31	0.67
	219.1	0	33.63	1
	222.1	0	32.44	1
	226.0	0	22.68	1
	228.9	4.66	17.22	0.79
	232.0	17.10	41.52	0.71
	235.0	12.86	33.52	0.72
	238.0	12.61	29.22	0.70
	241.0	0	22.06	1

Table S2. Summarized seasonal temperature, solar radiation, and R_{Bio}

	Pre-bloom	Bloom	Post-bloom
Temperature (°C)	-1.8 ± 2.2	-3.4 ± 3.4	3.3 ± 1.5
Radiation (W m^{-2})	51.3 ± 36.1	243.0 ± 63.4	222.5 ± 70.5
R_{Bio}	0.09 ± 0.07	0.32 ± 0.17	0.32 ± 0.13

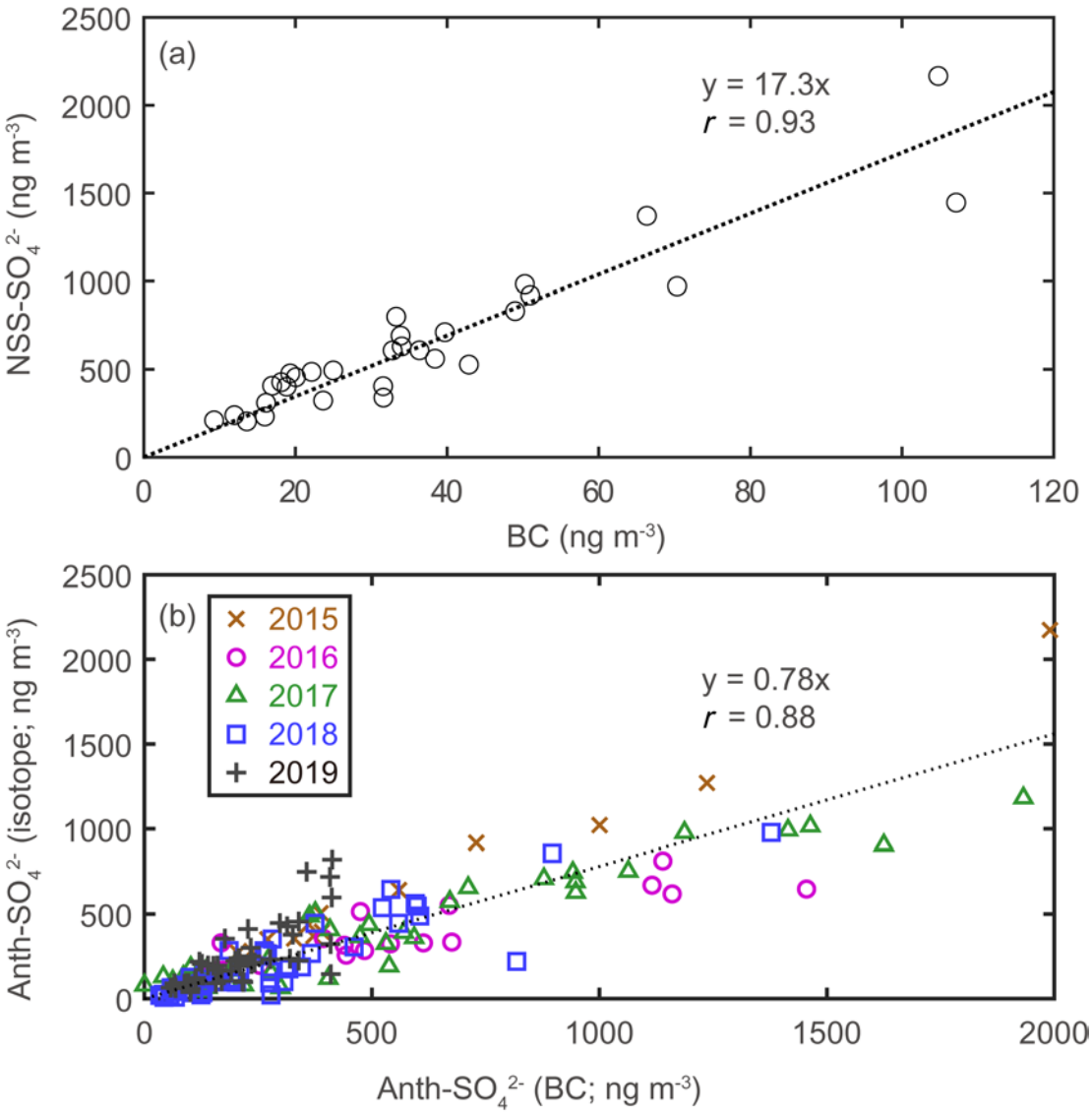

Figure S1: (a) Scatter plot of black carbon (BC) versus NSS-SO_4^{2-} samples collected in March to April (Bio-SO_4^{2-} < 20% of Total SO_4^{2-}; n = 23), (b) Scatter plot of Anth-SO_4^{2-} (calculated based on BC concentration) and Anth-SO_4^{2-} (stable isotope measurement results)

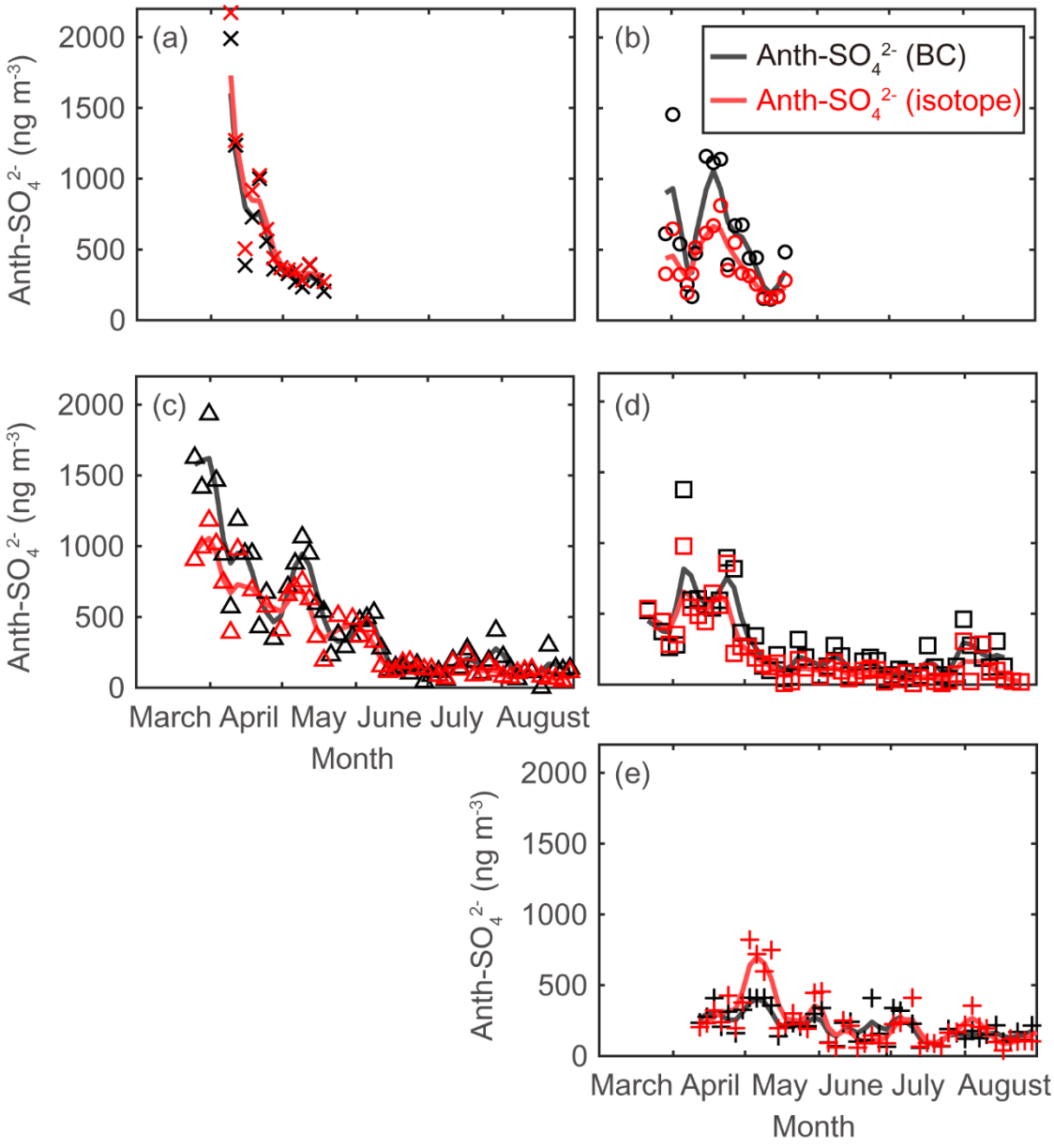

Figure S2: Anthropogenic sulfate concentration estimated by BC concentration (black) stable isotope analysis (red) for (a) 2015, (b) 2016, (c) 2017, (d) 2018, and (e) 2019.

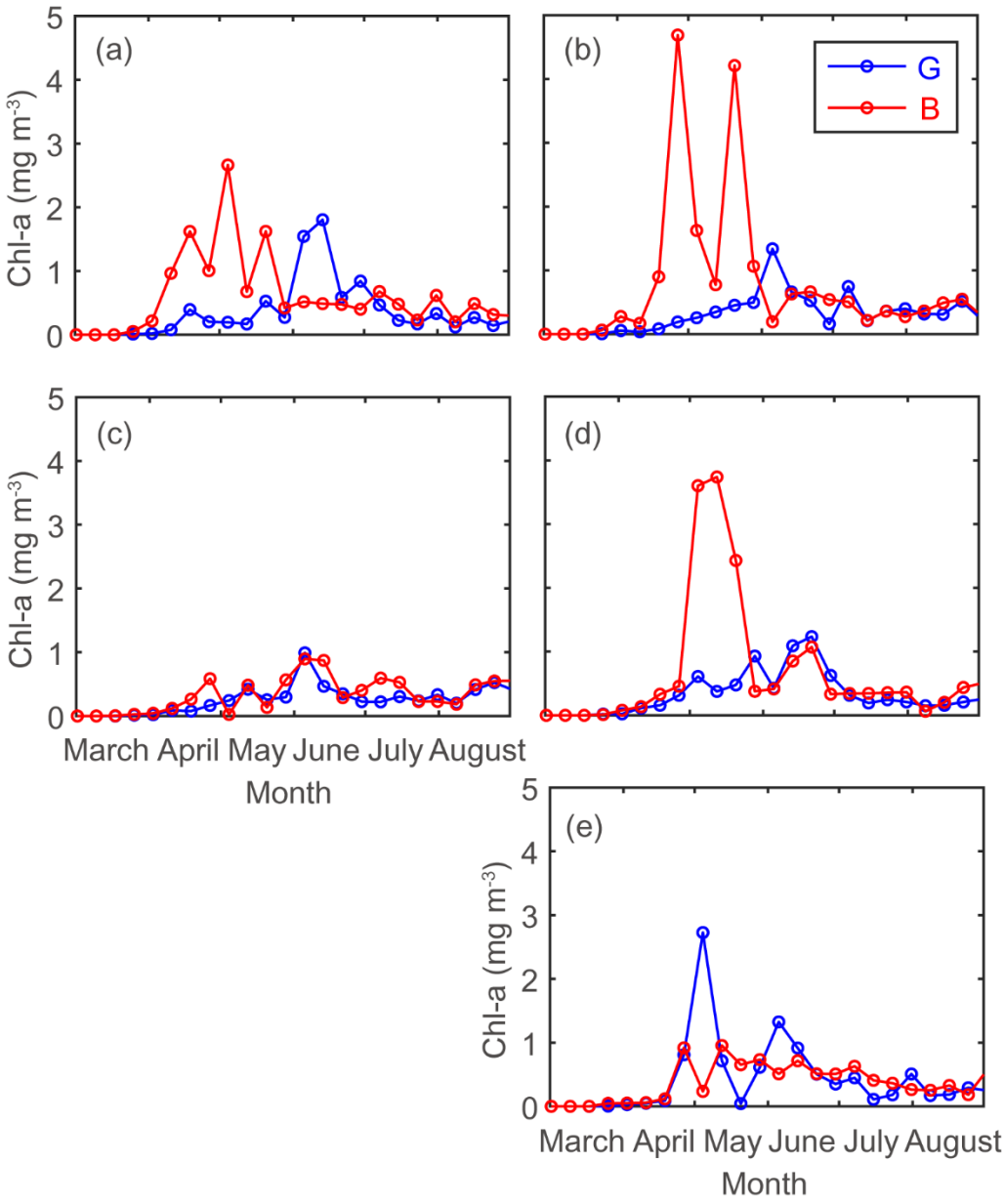

Figure S3: 8-day composite mean concentration of Chl-*a* in Greenland Sea (G; 70° N–80° N, 25° W–16° E; Blue) and Barents Sea (B; 70° N–80° N, 16° E–50° E; Red) for (a) 2015, (b) 2016, (c) 2017, (d) 2018, and (e) 2019.

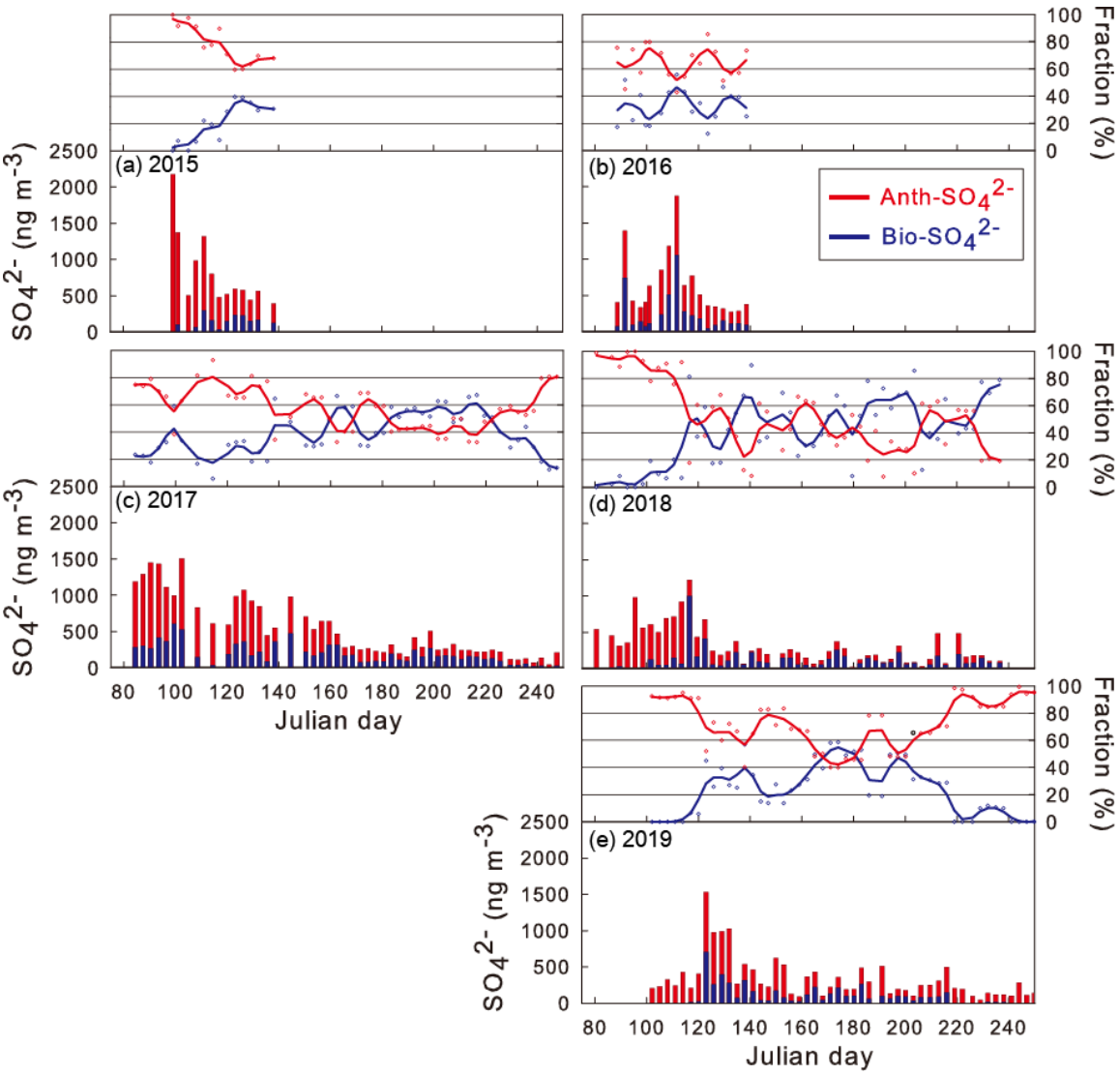

Figure S4: Bar plots showing the concentration of NSS-SO_4^{2-} aerosols (red: Anth-SO_4^{2-}; blue; Bio-SO_4^{2-}; ss-SO_4^{2-} not shown) for (a) 2015, (b) 2016, (c) 2017, (d) 2018, and (e) 2019.

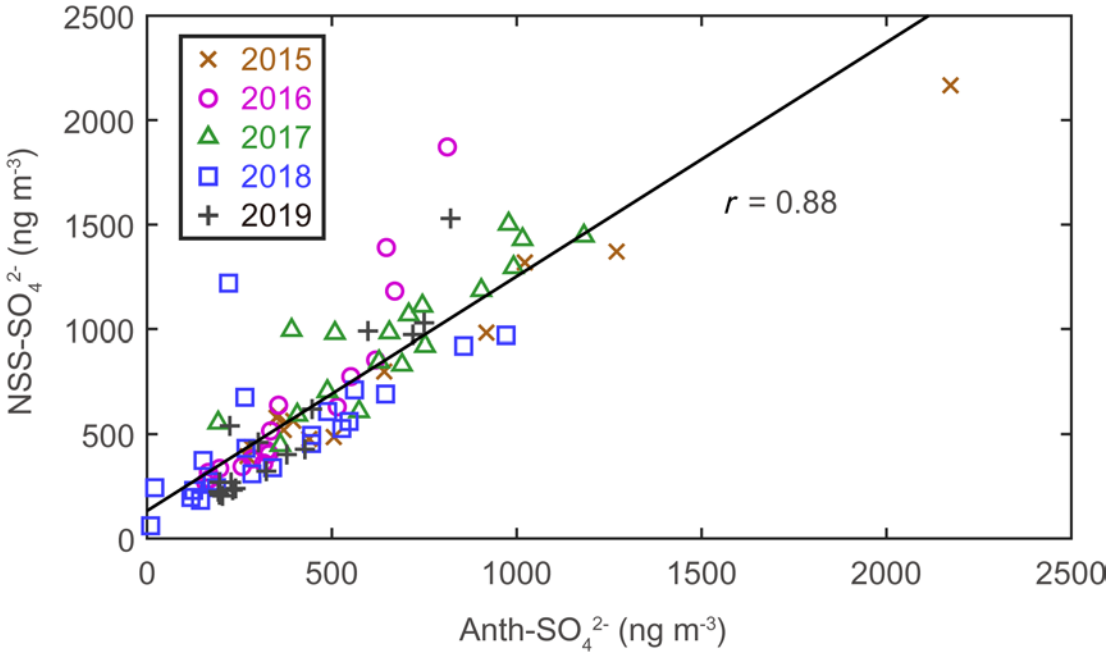

Figure S5: Scatter plot of NSS-SO_4^{2-} versus Anth-SO_4^{2-} from March to May for 2015, 2016, 2017, 2018, and 2019.

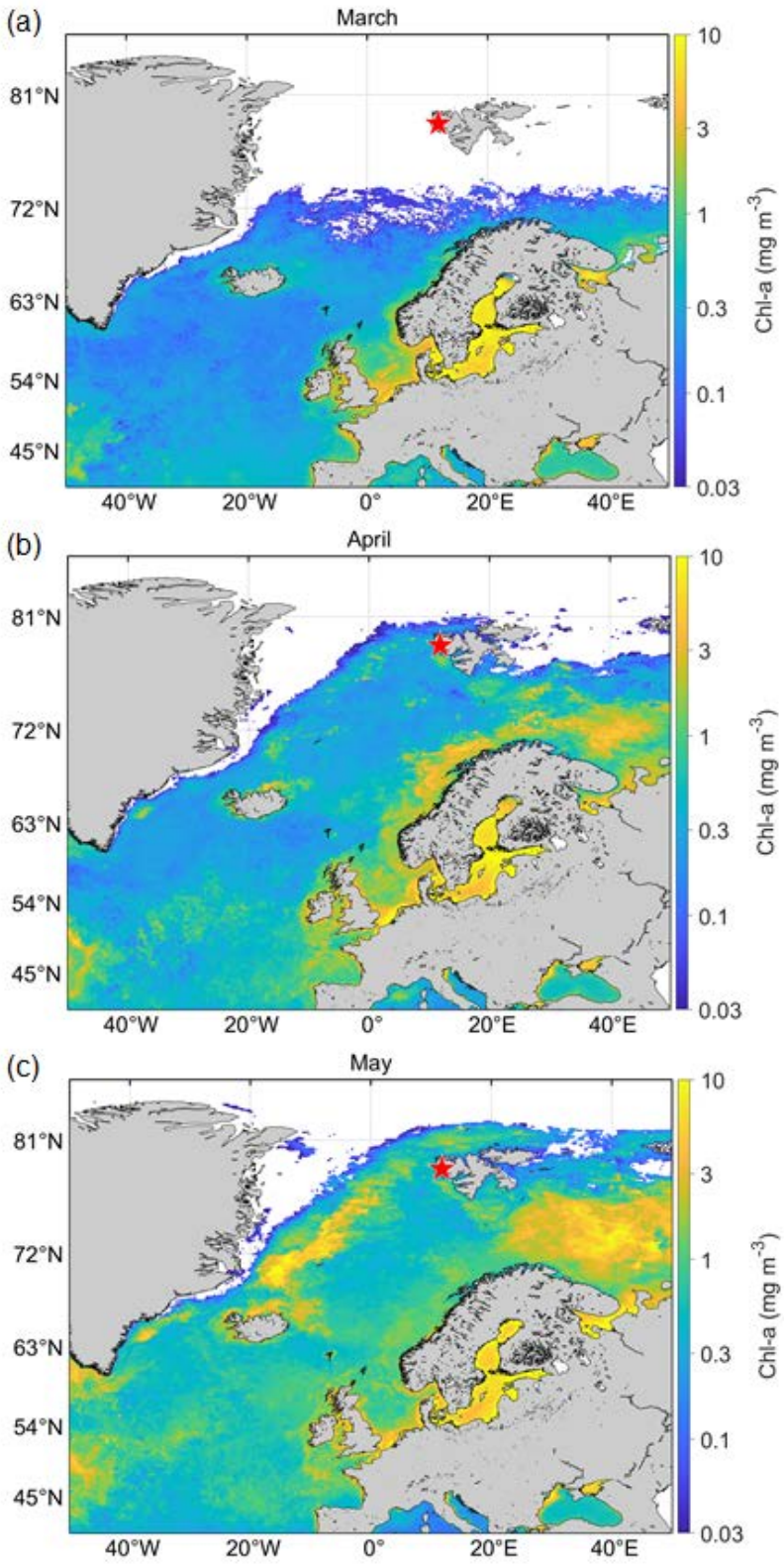

Figure S6: Monthly mean Chl-*a* concentration in the Arctic Ocean for 2015, 2016, 2017, 2018 and 2019. Red pentagram indicates the location of the sampling site.

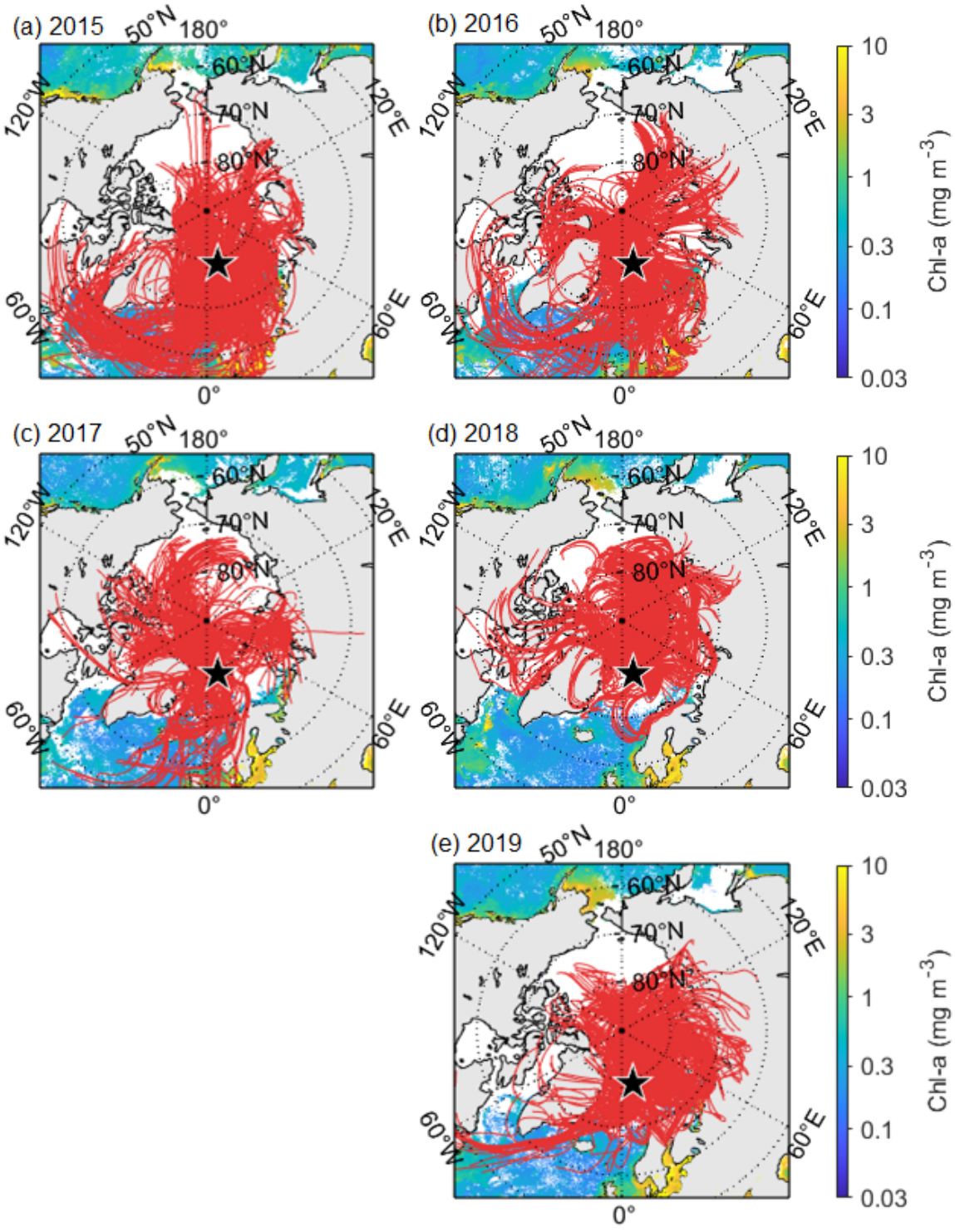

Figure S7: Monthly mean Chl-*a* concentration in each year layered with 5-day air mass back trajectories during March. Black pentagram indicates the location of the sampling site.

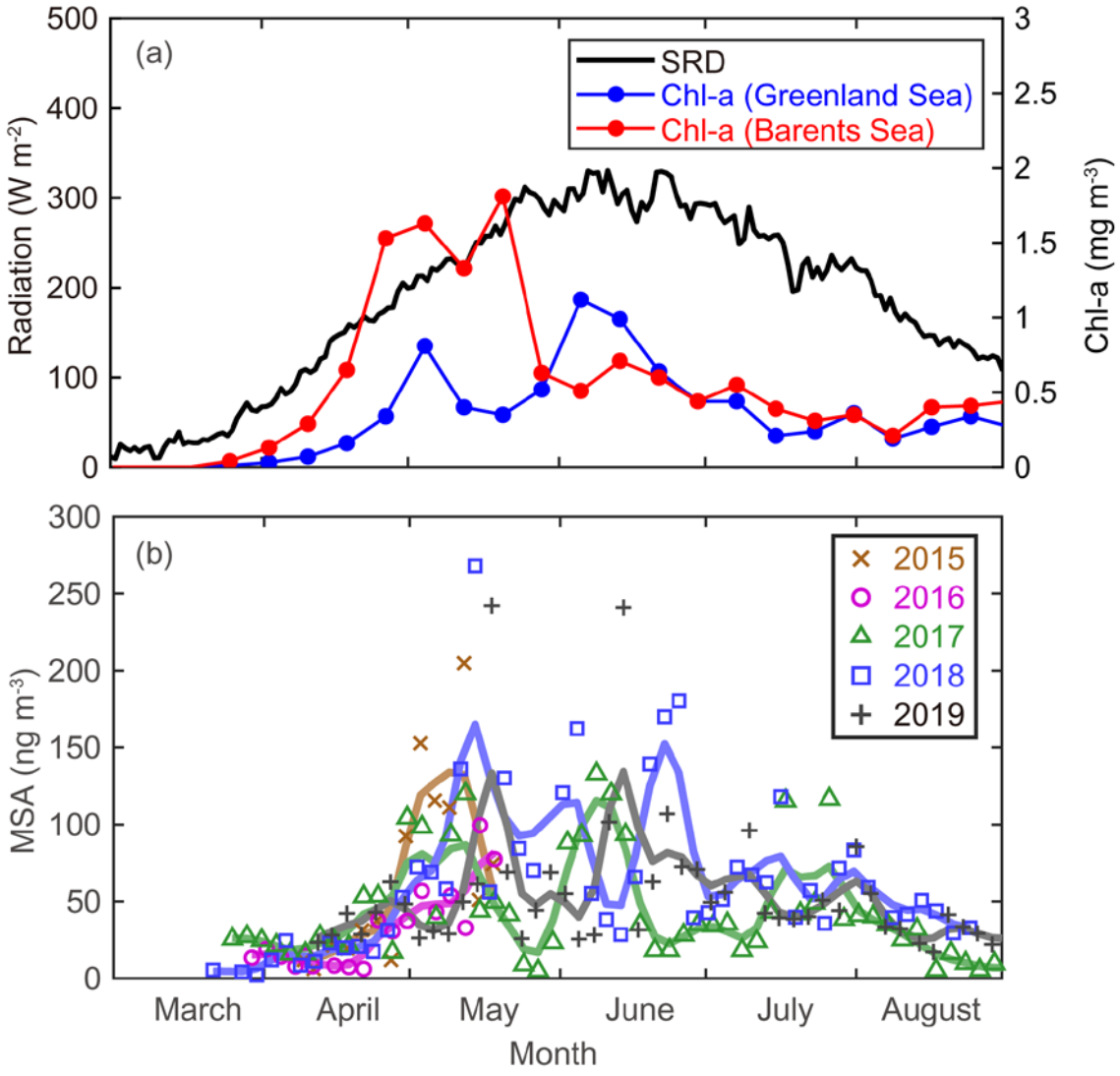

Figure S8: (a) Mean radiation and mean Chl-*a* concentration in Greenland and Barents Seas, (b) MSA concentration for 2015, 2016, 2017, 2018 and 2019.

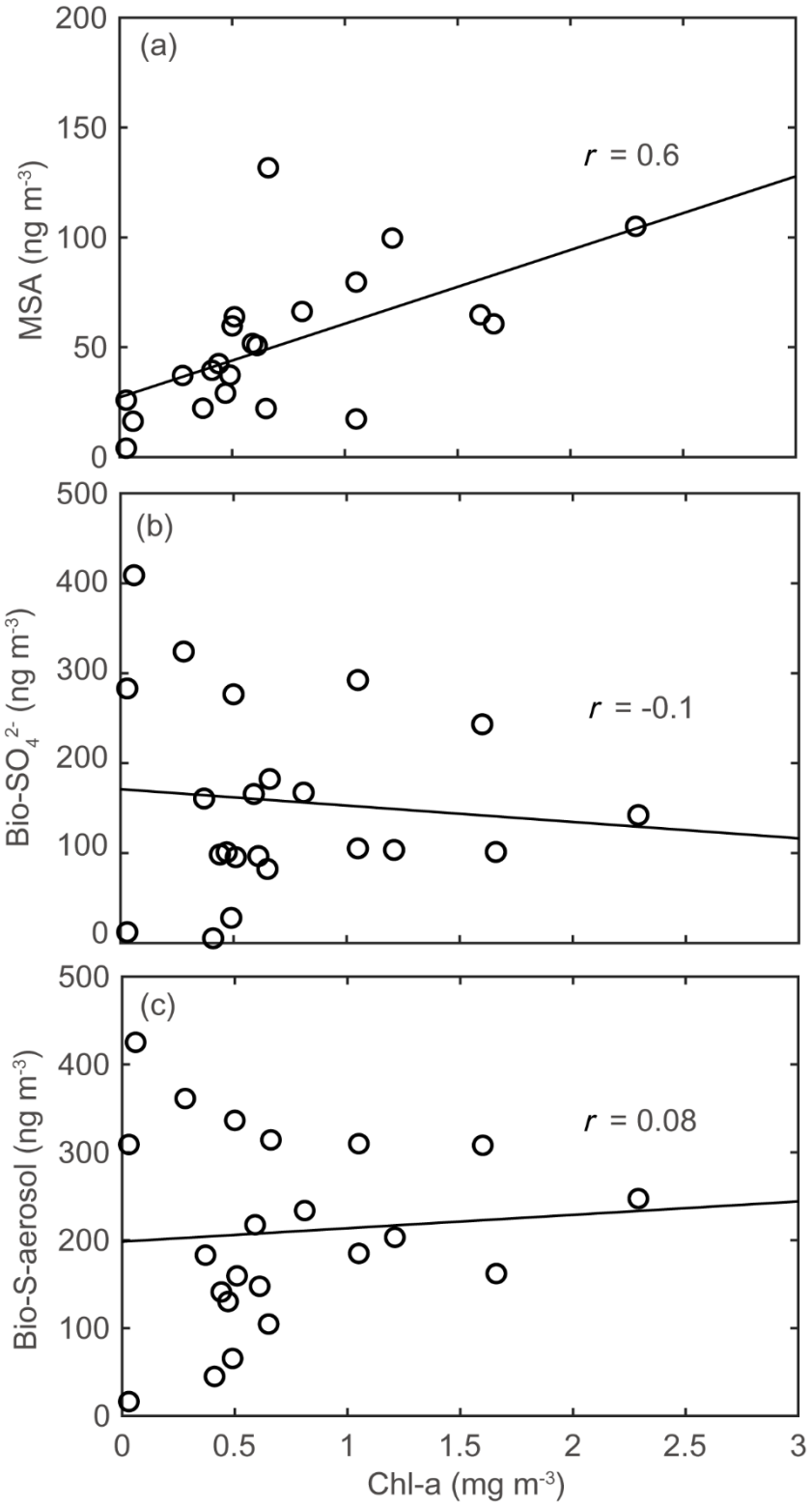

Figure S9: Scatter plot of monthly mean Chl-*a* versus (a) monthly mean MSA, (b) monthly mean Bio-SO_4^{2-}, and (b) monthly mean Bio-aerosol for 2015, 2016, 2017, 2018 and 2019.

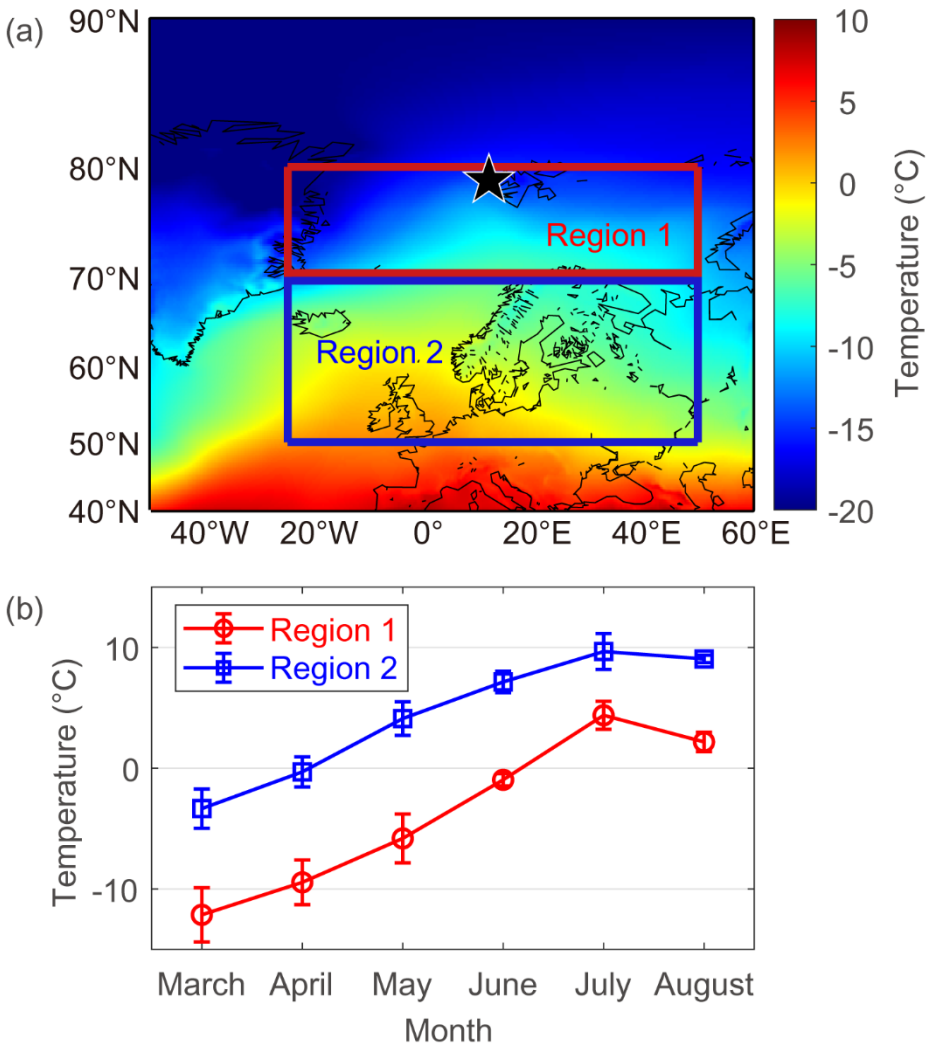

Figure S10: (a) Mean temperature map in March with ocean domains of Greenland & Barents Sea (Region 1; 70° N–80° N, 25° W–50° E), and North Atlantic & Norwegian Seas (Region 2; 50° N–70° N, 25° W–50° E), and (b) mean temperature at 900 hPa from European Centre for Medium-Range Weather Forecasts Reanalysis 5 in different ocean domains during 2015–2019, error bars represent 1σ for 2015, 2016, 2017, 2018 and 2019, respectively.

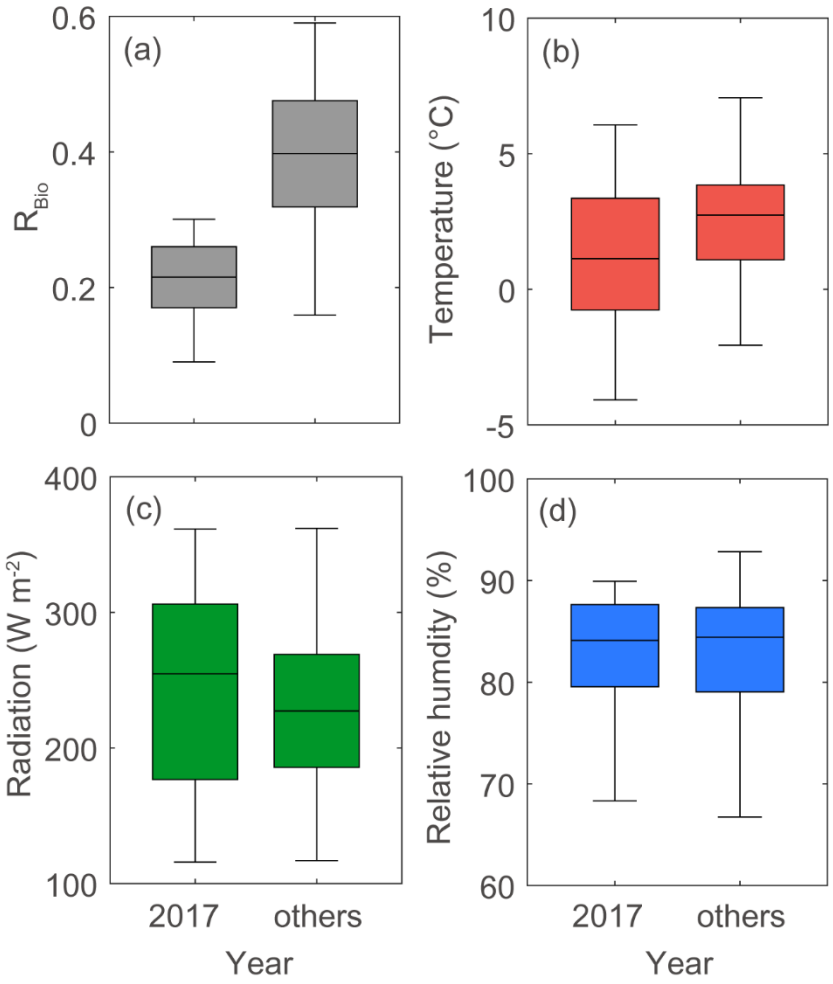

Figure S11: Box plot of (a) R_{Bio}, (b) air mass temperature, (c) radiation, (d) relative humidity during post-bloom period. Meteorological factors were calculated for air masses has been subject to in the 5 days prior to reaching the measurement site at Svalbard. Solid line represents median of each data in box plot.

References

Bates, T. S., Calhoun, J. A., and Quinn, P. K.: Variations in the methanesulfonate to sulfate molar ratio in submicrometer marine aerosol particles over the South Pacific Ocean, J. Geophys. Res.-Atmos., 97(D9), 9859–9865, https://doi.org/10.1029/92JD00411, 1992b.

Chen, L., Wang, J., Gao, Y., Xu, G., Yang, X., Lin, Q., and Zhang, Y.: Latitudinal distributions of atmospheric MSA and MSA/nss-SO_4^{2-} ratios in summer over the high latitude regions of the Southern and Northern Hemispheres, J. Geophys. Res., 117, D10306, https://doi.org/10.1029/2011JD016559, 2012.

Gong, S. L., Zhao, T. L., Sharma, S., Toom-Sauntry, D., Lavoué, D., Zhang, X. B., Leaitch, W. R., and Barrie, L. A.: Identification of trends and interannual variability of sulfate and black carbon in the Canadian High Arctic: 1981–2007, J. Geophys. Res.-Atmos., 115(D7), D07305, https://doi.org/10.1029/2009JD012943, 2010.

Hynes, A. J., Wine, P. H., and Semmes, D. H.: Kinetics and mechanism of hydroxyl reactions with organic sulfides, J. Phys. Chem., 90(17), 4148−4156, https://doi.org/10.1021/j100408a062, 1986.

Legrand, M., and Pasteur, E. C.: Methane sulfonic acid to non-sea-salt sulfate ratio in coastal Antarctic aerosol and surface snow, J. Geophys. Res.-Atmos., 103(D9), 10991−11006, https://doi.org/10.1029/98JD00929, 1998.

Li, S. M., and Barrie, L. A.: Biogenic sulfur aerosol in the Arctic troposphere: 1. Contributions to total sulfate, J. Geophys. Res.-Atmos., 98(D11), 20613−20622, https://doi.org/10.1029/93JD02234, 1993.

Li, S. M., Barrie, L. A., Talbot, R. W., Harriss, R. C., Davidson, C. I., and Jaffrezo, J. L.: Seasonal and geographic variations of methanesulfonic acid in the Arctic troposphere, Atmos. Environ. A.-Gen., 27(17-18), 3011−3024, https://doi.org/10.1016/0960-1686(93)90333-T, 1993.

Lin, C. T., Baker, A. R., Jickells, T. D., Kelly, S., and Lesworth, T.: An assessment of the significance of sulphate sources over the Atlantic Ocean based on sulphur isotope data, Atmos. Environ., 62, 615–621, https://doi.org/10.1016/j.atmosenv.2012.08.052, 2012.

Massling, A., Nielsen, I. E., Kristensen, D., Christensen, J. H., Sørensen, L. L., Jensen, B., Nguyen, Q. T., Nøjgaard, J. K., Glasius, M. and Skov, H.: Atmospheric black carbon and sulfate concentrations in Northeast Greenland, Atmos. Chem. Phys., 15(16), 9681–9692, https://doi.org/10.5194/acp-15-9681-2015, 2015.

Norman, A. L., Barrie, L. A., Toom-Sauntry, D., Sirois, A., Krouse, H. R., Li, S. M., and Sharma, S.: Sources of aerosol sulphate at Alert: Apportionment using stable isotopes, J. Geophys. Res.-Atmos., 104, 11619–11631, https://doi.org/10.1029/1999JD900078, 1999.

Shaw, G. E.: The Arctic haze phenomenon, B. Meteorol. Soc., 76(12), 2403–2414, https://doi.org/10.1175/1520-0477(1995)076<2403:TAHP>2.0.CO;2, 1995.

Udisti, R., Bazzano, A., Becagli, S., Bolzacchini, E., Caiazzo, L., Cappelletti, D., Ferrero, L., Frosini, D., Giardi, F., Grotti, M., Lupi, A., Malandrino, M., Mazzola, M., Moroni, B., Severi, M., Traversi, R.,

Viola, A., and Vitale, V.: Sulfate source apportionment in the Ny Ålesund (Svalbard Islands) Arctic aerosol, Rend. Lincei, 27, S85–S94, https://doi.org/10.1007/s12210-016-0517-7, 2016.

Yin, F., Grosjean, D., and Seinfeld, J. H.: Photooxidation of dimethyl sulfide and dimethyl disulfide. I: Mechanism development, J. Atmos. Chem., 11(4), 309−364, https://doi.org/10.1007/BF00053780, 1990.